

# HI OBSERVATIONS OF MAJOR-MERGER PAIRS AT Z = 0: ATOMIC GAS AND STAR FORMATION

PEI ZUO<sup>1,4</sup>, CONG K. XU<sup>2,1</sup>, MIN S. YUN<sup>3</sup>, UTE LISENFELD<sup>5</sup>, DI LI<sup>1,4,6</sup>, AND CHEN CAO<sup>7, 8</sup>

<sup>1</sup> National Astronomical Observatories, Chinese Academy of Sciences, Beijing 100101, China

<sup>2</sup> Chinese Academy of Sciences South America Center for Astronomy, China-Chile Joint Center for Astronomy, Camino El Observatorio 1515, Las Condes, Santiago, Chile

<sup>3</sup> Department of Astronomy, University of Massachusetts, Amherst, MA 01003, USA

<sup>4</sup> University of Chinese Academy of Sciences, Beijing 100049, China

<sup>5</sup> Departamento de Física Teórica y del Cosmos, Universidad de Granada, Spain and Instituto Carlos I de Física Teórica y Computacional, Facultad de Ciencias, 18071 Granada, Spain

<sup>6</sup> CAS Key Laboratory of FAST, NAOC, Chinese Academy of Sciences, Beijing, 100101, China

<sup>7</sup> School of Space Science and Physics, Shandong University, Weihai, Shandong 264209, China

<sup>8</sup> Shandong Provincial Key Laboratory of Optical Astronomy & Solar-Terrestrial Environment, Weihai, Shandong 264209, China

*Draft version August 13, 2018*

## ABSTRACT

We present a study of the HI gas content of a large K-band selected sample of 88 close major-merger pairs of galaxies (H-KPAIR) which were observed by *Herschel*. We obtained the 21 cm HI fine-structure emission line data for a total of 70 pairs from this sample, by observing 58 pairs using the Green Bank Telescope (GBT) and retrieving the HI data for an addition 12 pairs from the literature. In this HI sample, 34 pairs are spiral-spiral (S+S) pairs, and 36 are spiral-elliptical (S+E). Based on these data, we studied the HI-to-stellar mass ratio, the HI gas fraction and the HI star formation efficiency ( $SFE_{\text{HI}} = \text{star formation rate}/M_{\text{HI}}$ ) and searched for differences between S+S and S+E pairs, as well as between pairs with and without signs for merger/interaction. Our results showed that the mean HI-to-stellar mass ratio of spirals in these pairs is  $= 7.6 \pm 1.0\%$ , consistent with the average HI gas fraction of spiral galaxies in general. The differences in the HI gas fraction between spirals in S+S and in S+E pairs, and between spirals in pairs with and without signs of merger/interaction are insignificant ( $< 1\sigma$ ). On the other hand, the mean  $SFE_{\text{HI}}$  of S+S pairs is  $\sim 4.6\times$  higher than that of S+E pairs. This difference is very significant ( $\sim 4\sigma$ ) and is the main result of our study. There is no significant difference in the mean  $SFE_{\text{HI}}$  between galaxies with and without signs of merger/interaction. The mean  $SFE_{\text{HI}}$  of the whole pair sample is  $10^{-9.55 \pm 0.09} \text{ yr}^{-1}$ , corresponding to a HI consumption time of  $3.5 \pm 0.7$  Gyrs.

*Keywords:* galaxies: interactions — galaxies: evolution — galaxies: star formation

## 1. INTRODUCTION

It has been well documented that galaxy-galaxy interaction can induce enhanced star formation (Larson & Tinsley 1978; Keel et al. 1985; Kennicutt et al. 1987; Bushouse et al. 1988; Telesco et al. 1988; Sulentic 1989; Xu & Sulentic 1991; Barton et al. 2000; Lambas et al. 2003; Alonso et al. 2004; Nikolic et al. 2004; Li et al. 2008; Ellison et al. 2008; Xu et al. 2010). More recently, Scudder et al. (2012) and Patton et al. (2013) found that wide galaxy pairs with separation as large as  $\sim 80$  kpc still

show significant star formation rate (SFR) enhancement at  $\sim 40\%$  level. Early studies (Hummel 1981; Haynes & Herter 1988; Bergvall et al. 2003) that failed to detect SFR enhancement in interacting galaxies may have suffered from biases in selecting the interacting galaxy sample and the control sample (Xu et al. 2010; Ellison et al. 2010, c.f.).

Of particular interest are close (separation  $\leq 20 h^{-1}$  kpc) major mergers of galaxies of nearly equal mass (primary-to-secondary mass ratio  $\lesssim 3$ ). Most extreme starbursts such as ultra-luminous infrared galaxies (ULIRGs) are close major mergers (Sanders & Mirabel 1996; Dasyra et al. 2006). For a sample of K-band selected close major-merger pairs, IR observations carried out using *Spitzer* (Xu et al. 2010) and *Herschel* (Cao et al. 2016) found that in these pairs the average specific SFR ( $sSFR = SFR/M_{\text{star}}$ ) in spirals is a factor of  $\gtrsim 2$  higher than that of their counterparts in the control sample. Furthermore, spirals in spiral-spiral pairs (S+S pairs) are strongly enhanced with the mean  $sSFR \gtrsim 3$  times higher than that of control galaxies, but spirals in mixed spiral-elliptical pairs (S+E pairs) do not show any significant SFR enhancement compared to the control galaxies. Using *WISE* and *Herschel* data, Domingue et al. (2016) also found that spirals in S+S pairs exhibit significant enhancements in interstellar

Email: peizuo@nao.cas.cn, congxu@nao.cas.cn

<sup>1</sup> National Astronomical Observatories, Chinese Academy of Sciences, Beijing 100101, China

<sup>2</sup> South American Center for Astronomy, CAS, Camino El Observatorio 1515, Las Condes, Santiago, Chile

<sup>3</sup> Department of Astronomy, University of Massachusetts, Amherst, MA 01003, USA

<sup>4</sup> University of Chinese Academy of Sciences, Beijing 100049, China

<sup>5</sup> Departamento de Física Teórica y del Cosmos, Universidad de Granada, Spain and Instituto Carlos I de Física Teórica y Computacional, Facultad de Ciencias, 18071 Granada, Spain

<sup>6</sup> CAS Key Laboratory of FAST, NAOC, Chinese Academy of Sciences, Beijing, 100101, China

<sup>7</sup> School of Space Science and Physics, Shandong University, Weihai, Shandong 264209, China

<sup>8</sup> Shandong Provincial Key Laboratory of Optical Astronomy & Solar-Terrestrial Environment, Weihai, Shandong 264209, China

radiation field and dust temperature while spirals in S+E pairs do not.

Why is the sSFR enhancement of spirals in mixed S+E pairs different from that of spirals in S+S pairs? If the enhancement is purely due to gravitational tidal effect, then the spirals in S+E pairs should behave similarly to spirals in S+S pairs unless the former have systematically less cold gas (i.e. the fuel for star formation) than the latter. This possibility has been tested by [Cao et al. \(2016\)](#). Using fluxes in six *Herschel* bands (70, 100, 160, 250, 350, and 500  $\mu\text{m}$ ), they estimated dust mass ( $M_{\text{dust}}$ ) and, assuming a constant dust-to-gas mass ratio, total gas mass ( $M_{\text{gas}}$ ) for the paired spirals. They found only marginal evidence for spirals in S+E pairs having slightly lower gas content than those in S+S pairs ( $\delta\log(M_{\text{gas}}/M_{\text{star}}) = -0.14 \pm 0.10$ ). It appears that the difference between the sSFR enhancements of spirals in mixed S+E pairs and of those in S+S pairs is mainly due to their different star formation efficiency ( $\text{SFE} = \text{SFR}/M_{\text{gas}}$ ), suggesting significant roles for non-tidal effects (e.g. collision between gas in two galaxies) in the interaction induced star formation.

In this paper, we represent a study on the HI gas content of pairs. The main science goal is to constrain the relation between HI gas content and SFR enhancement, and check the consistency with the relation between gas content (estimated using the dust mass) and SFR enhancement obtained in the *Herschel* study ([Cao et al. 2016](#)). In section 2, 3 and 4, we describe the sample, GBT observations, and data reduction. Literature data are described in Section 5. Main results are presented in Section 6. Section 7 is devoted to discussions. Section 8 is the summary. Through out this paper, we adopt the  $\Lambda$ -cosmology with  $\Omega_m = 0.3$  and  $\Omega_\Lambda = 0.7$ , and  $H_0 = 70$  ( $\text{km s}^{-1} \text{Mpc}^{-1}$ ).

## 2. THE H-KPAIR SAMPLE

The KPAIR is an unbiased and large sample of 170 close major-merger galaxy pairs selected in the K-band, from cross matches between the Two Micron All Sky Survey (2MASS) and the Sloan Digital Sky Survey (SDSS)-DR5 galaxies ([Domingue et al. 2009](#)). The parent sample includes 77,451 galaxies of  $K_s \leq 13.5$  mag, with a sky coverage of 5800  $\text{deg}^2$  and redshift completeness of 86%. The selection criteria are: (1)  $K_s$  magnitude of the primary is not fainter than 12.5; (2) at least one component has a measured redshift; (3) if both components have measured redshifts, the velocity difference is not larger than 1000  $\text{km s}^{-1}$ ; (4) the  $K_s$  difference between the two galaxies is not larger than 1 mag; (5) the projected separation is in the range of  $5 \text{ h}^{-1} \text{ kpc} \leq r \leq 20 \text{ h}^{-1} \text{ kpc}$ . When only one component has a measured redshift, the separation is calculated according to that redshift and the angular separation of the components. Visual inspections, complemented by results of an automatic algorithm, classified 62 pairs as S+S, 56 as S+E, and 52 as E+E.

The H-KPAIR sample ([Cao et al. 2016](#)) includes all S+S and S+E pairs in the original KPAIR sample that have (1) measured redshifts for both components, (2) relative velocity  $< 500 \text{ km s}^{-1}$ , and (3) pair recession velocity  $< 2000 \text{ km s}^{-1}$ . It contains 88 pairs (44 S+S and 44 S+E). We did some of these comparison in [Xu et al.](#)

(2010) and [Cao et al. \(2016\)](#). We will do a comprehensive comparison between S+S and S+E in a future paper.

## 3. OBSERVATIONS

For 67 pairs, the 21 cm HI fine-structure line observations were carried out using the National Radio Astronomy Observatory (NRAO)<sup>9</sup> Robert C. Byrd Green Bank 110-m Telescope (GBT)<sup>10</sup> Spectrometer in the L-band (1.15-1.73 GHz) between 2012 August and 2013 January. For each object, the data were collected in  $\sim 2$  hrs on-off source pairs with 12.5 MHz bandwidth. The two spectral windows were centered at the same frequency (1420.4058 MHz). Using 9-level sampling and two IFs, the observations provide 1.5 kHz ( $0.3 \text{ km s}^{-1}$ ) spectral resolution for the dual polarization L-band system. The beam size is  $9' \times 9'$ . GBT has a well-calibrated structure and a stable gain at the 21 cm wavelength. We observed 3C 286 as the primary flux calibrator to monitor the instrumental performance. This observation of a bright calibration source verified the stability of the telescope gain factor. As a test, we also observed 5 nearby normal galaxies: NGC895, NGC2718, NGC3027, UGC10014, and NGC6140. Comparisons with literature show a systematic difference of  $\sim 15\%$  between our measurements and data in the literature (see Appendix A), suggesting a minor deviation in the calibration. This shall not affect our main conclusions significantly.

## 4. DATA REDUCTION

The HI spectra were reduced using GBTIDL ([Manganian et al. 2006](#)). We used the Jy/K calibration to convert the HI line fluxes to the units of Jy, applying an atmospheric opacity of 0.008 and aperture efficiency of 0.71. The scans and channels with Radio Frequency Interferences (RFIs) were flagged. For each polarization, the data were accumulated and averaged together. A polynomial of the order of 3 - 8 was used to fit the baseline over a range of  $\approx 4500$  channels for every pair. The Hanning-smoothed and then decimated spectra were used to subtract the baseline. The velocity resolution is  $\sim 30 \text{ km s}^{-1}$  per channel after boxcar smoothing. The two polarizations were then averaged together to produce the full intensity spectra shown in Figure 1.

Some observations were significantly affected by RFIs. For 9 pairs (J0913+4742, J0926+0447, J1010+5440, J1020+4831, J1137+4728, J1148+3547, J1205+0135, J1505+3427, J1628+4109), the RFIs are so severe that no informative signals could be extracted from the data. The pairs are excluded from our analysis. Forty-six targets are detected with the HI 21 cm emission peak  $> 3\sigma$ . Their HI masses were calculated using the relationship of  $M_{\text{HI}} = 2.36 \times 10^5 D^2 (S\Delta V) M_\odot$  ([Condon & Ransom 2016](#)), where  $D$  is the luminosity distance in Mpc and  $S\Delta V$  is the velocity integrated HI flux density in  $\text{Jy km s}^{-1}$ . The HI velocity range was visually decided, with the constraint that the center is within  $\pm 400 \text{ km s}^{-1}$  from the system velocity (optical) of the

<sup>9</sup> The National Radio Astronomy Observatory is a facility of the National Science Foundation operated under cooperative agreement by Associated Universities, Inc.

<sup>10</sup> The Green Bank Observatory is a facility of the National Science Foundation operated under cooperative agreement by Associated Universities, Inc.

target. The HI masses of the 12 undetected pairs were calculated based on the  $3\sigma$  upper limits of the spectral line with assumed line-width of  $\sim 800 \text{ km s}^{-1}$ . The error was estimated by the quadratic sum of the 10% systematic uncertainty (mostly due to the calibration and the baseline subtraction error) and the measured rms noise. We also measured the mean HI velocity (weighted by signal) and the  $W_{20}$  of the spectral line for detected pairs.

For the 46 detected pairs, we visually inspected their SDSS images and found that 22 have neighboring spiral galaxies with redshifts inside the bandwidth of the HI observation and locations within  $10'$  from the pair center (Figure B1 in Appendix B). We performed our search down to the limit of 17.71 mag ( $i$ -band), 18.35 mag ( $g$ -band) and 17.78 mag ( $r$ -band). All spiral galaxies in the search radius and brighter than these limits had observed redshifts. As the beam of GBT is  $9'$ , contamination due to blending could be significant for these sources, therefore a correction was carried out based on the algorithm developed by Zhang et al. (2009). Details about the contamination correction are presented in Appendix B. Most of the neighboring galaxies cause minor corrections. The average and the range of the factor by which  $M_{\text{HI}}$  was changed due to the correction are 1.26 and 1.03-1.84, respectively. Also, as a test for the algorithm, we found that for paired galaxies in our sample the ratio between estimated and observed HI mass is consistent with being unity ( $0.8 \pm 0.2$ ). The HI mass after this correction was listed as  $M_{\text{HI},c}$  in column (7) in Table 1.

## 5. LITERATURE DATA

The 21 pairs in H-KPAIR that we did not observe with GBT were covered by previous HI emission line observations. However, detailed inspections showed that among them 9 pairs (J0915+4419, J1015+0657, J1150+1444, J1211+4039, J1219+1201, J1429+3534, J1506+0346, J1514+0403, J1608+2529) are in galaxy groups and the HI observations were not pointed to the pairs but to neighboring galaxies in the same group, as shown in Figure B1. Therefore their HI mass are too uncertain and they are excluded from our analysis. For each of the remaining 12 pairs, the HI data collected from the literature are listed in Table 2. No neighboring spiral galaxies that can cause significant HI contaminations were found for these pairs (Figure B1 in Appendix B).

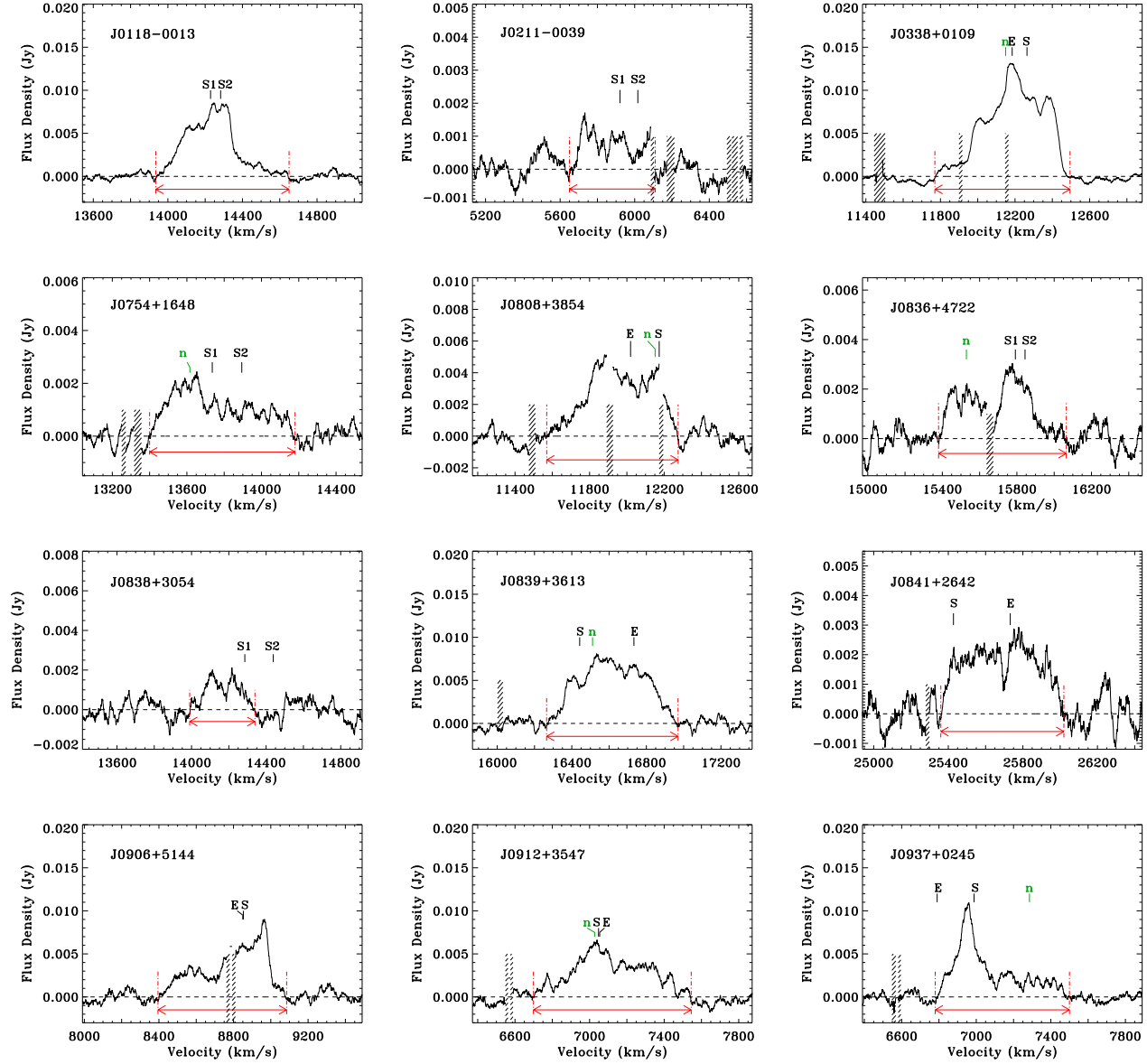


**Figure 1.** HI profiles of major-merger pairs observed with 100m GBT. Optical redshifts of individual galaxies are marked with short vertical lines on the observed spectra. For S+E pairs, “S” and “E” are for the S and E components, respectively. For the S+S pairs, “S1” represents the western galaxy and “S2” represents the eastern one. Short vertical lines in green denoted by n, n1, n2, ..., mark the optical redshifts of neighboring galaxies in the beam. The regions with hash marks are frequencies where the data are affected by RFI spikes. The region between the two red dot-dash lines represents the range of the intensity flux integration. (The complete figure set (5 plots) is available.)

**Table 1**  
Pairs in GBT observations.

| (1)<br>Pair ID<br>(H-KPAIR) | (2)<br>R.A.<br>(J2000) | (3)<br>decl.<br>(J2000) | (4)<br>$V_{\text{optical}}$<br>( $\text{km s}^{-1}$ ) | (5)<br>$V_{\text{HI}}$<br>( $\text{km s}^{-1}$ ) | (6)<br>$M_{\text{HI}}$<br>( $10^9 M_{\odot}$ ) | (7)<br>$M_{\text{HI},c}$<br>( $10^9 M_{\odot}$ ) | (8)<br>$W20$<br>( $\text{km s}^{-1}$ ) | (9)<br>$100 \times M_{\text{dust}}$<br>( $10^9 M_{\odot}$ ) | (10)<br>$M_{\text{star}}$<br>( $10^9 M_{\odot}$ ) | (11)<br>SFR<br>( $M_{\odot} \text{ yr}^{-1}$ ) | (12)<br>Type |
|-----------------------------|------------------------|-------------------------|---|--|--|--|--|---|---|--|--------------|
| J0118-0013                  | 01:18:34.9             | -00:13:50               | 14160   | 14235  | 22.64 ± 2.29                                   |  | 389.38                                 | 26.51   | 140.17  | 61.83  | SS           |
| J0211-0039                  | 02:11:07.4             | -00:39:17               | 5970  | 5874   | 0.45 ± 0.06                                    |  | *301.24                                | 4.54  | 76.05   | 2.95   | SS           |
| J0338+0109                  | 03:38:12.6             | +01:09:55               | 12240   | 12194  | 29.76 ± 2.98                                   | 21.72  | 491.08                                 | 13.49   | 50.12   | 5.02   | SE           |
| J0754+1648                  | 07:54:32.1             | +16:48:28               | 13812   | 13741  | 8.42 ± 0.90                                    | 7.24   | *612.13                                | 42.90   | 232.46  | 30.02  | SS           |
| J0808+3854                  | 08:08:34.7             | +38:54:52               | 12040   | 11964  | 12.21 ± 1.26                                   | 11.21  | 519.60                                 | 2.29  | 51.29   | 1.35   | SE           |
| J0836+4722                  | 08:36:45.4             | +47:22:14               | 15768   | 15684  | 11.03 ± 1.28                                   | 6.00   | 507.72                                 | <4.95   | 230.40  | 0.82   | SS           |
| J0838+3054                  | 08:38:17.8             | +30:54:57               | 14344   | 14167  | 2.52 ± 0.54                                    |  | 294.54                                 | 4.26  | 162.11  | 4.21   | SS           |
| J0839+3613                  | 08:39:00.5             | +36:13:10               | 16569   | 16619  | 46.29 ± 4.70                                   | 44.05  | 551.70                                 | 13.49   | 81.28   | 1.91   | SE           |
| J0841+2642                  | 08:41:50.1             | +26:42:52               | 25600   | 25685  | 8.46 ± 2.10                                    |  | 617.95                                 | 4.90  | 257.04  | 1.43   | SE           |
| J0906+5144                  | 09:06:03.9             | +51:44:24               | 8737  | 8795   | 8.30 ± 0.87                                    |  | 538.90                                 | 6.92  | 39.81   | 1.26   | SE           |
| J0912+3547                  | 09:12:36.6             | +35:47:32               | 7056  | 7112   | 5.98 ± 0.62                                    | 5.61   | 629.60                                 | <0.37   | 17.38   | <0.04  | SE           |
| J0937+0245                  | 09:37:44.6             | +02:45:14               | 6890  | 7056   | 5.23 ± 0.55                                    | 5.01   | *275.36                                | 23.44   | 144.54  | 9.83   | SE           |
| J1022+3446                  | 10:22:56.5             | +34:46:51               | 16761   | 16733  | 15.25 ± 1.75                                   |  | 572.21                                 | 7.59  | 143.43  | 5.65   | SS           |
| J1023+4220                  | 10:23:36.7             | +42:20:55               | 13659   | 13651  | 32.74 ± 3.33                                   | 28.44  | *451.30                                | 15.11   | 100.05  | 13.36  | SS           |
| J1027+0114                  | 10:27:29.6             | +01:15:02               | 6670  | 6718   | 6.01 ± 0.62                                    | 5.63   | *139.39                                | 2.75  | 26.30   | 1.91   | SE           |
| J1032+5306                  | 10:32:53.2             | +53:06:50               | 19186   | ...  | <3.06  |  | ...                                    | <2.85   | 104.71  | 1.03   | SE           |
| J1033+4404                  | 10:33:30.7             | +44:04:27               | 15658   | 15791  | 24.21 ± 2.62                                   |  | *432.10                                | 34.32   | 216.94  | 18.53  | SS           |
| J1036+5447                  | 10:36:43.4             | +54:47:42               | 13743   | ...  | <2.39  |  | ...                                    | <1.93   | 60.26   | <0.17  | SE           |
| J1039+3904                  | 10:39:24.3             | +39:04:53               | 13017   | ...  | <1.32  |  | ...                                    | 1.93  | 52.48   | <0.17  | SE           |
| J1045+3910                  | 10:45:24.9             | +39:10:09               | 7879  | ...  | <0.72  |  | ...                                    | 4.27  | 42.66   | 0.67   | SE           |
| J1051+5101                  | 10:51:44.1             | +51:01:25               | 7325  | ...  | <0.57  |  | ...                                    | <0.45   | 63.09   | <0.16  | SE           |
| J1059+0857                  | 10:59:58.9             | +08:57:28               | 18490   | ...  | <3.20  |  | ...                                    | <2.98   | 72.44   | <0.32  | SE           |
| J1101+5720                  | 11:01:43.6             | +57:20:19               | 14208   | 14130  | 7.90 ± 1.13                                    |  | 280.37                                 | <2.34   | 34.67   | <2.01  | SE           |
| J1106+4751                  | 11:06:50.1             | +47:51:10               | 19464   | 19516  | 47.27 ± 5.01                                   |  | 647.25                                 | 16.60   | 228.83  | 8.47   | SS           |
| J1120+0028                  | 11:20:47.3             | +00:28:10               | 7295  | 7308   | 7.81 ± 0.79                                    | 5.59   | 449.42                                 | 1.16  | 94.00   | 1.12   | SS           |
| J1125+0226                  | 11:25:17.1             | +02:26:54               | 14730   | 14713  | 20.91 ± 2.23                                   |  | 613.87                                 | 10.94   | 145.81  | 1.13   | SS           |
| J1127+3604                  | 11:27:33.8             | +36:04:01               | 10528   | 10397  | 14.87 ± 1.51                                   | 11.97  | 555.50                                 | 21.55   | 224.07  | 5.76   | SS           |
| J1144+3332                  | 11:44:03.8             | +33:32:20               | 9489  | 9519   | 4.64 ± 0.54                                    | 2.77   | 336.63                                 | 3.80  | 22.39   | 1.11   | SE           |
| J1150+3746                  | 11:50:13.7             | +37:46:20               | 16587   | 16491  | 39.70 ± 4.03                                   |  | 923.50                                 | 13.72   | 158.31  | 4.40   | SS           |
| J1154+4932                  | 11:54:23.0             | +49:32:48               | 21200   | ...  | <4.41  |  | ...                                    | 3.11  | 89.13   | <0.12  | SE           |
| J1202+5342                  | 12:02:04.8             | +53:42:40               | 19290   | 19269  | 12.57 ± 1.64                                   |  | *282.80                                | 10.72   | 75.86   | 1.78   | SE           |
| J1243+4405                  | 12:43:39.1             | +44:05:52               | 12412   | 12455  | 5.77 ± 0.67                                    |  | *255.70                                | 4.36  | 69.18   | 1.17   | SE           |
| J1252+4645                  | 12:52:51.1             | +46:45:28               | 18346   | 18246  | 5.80 ± 1.41                                    |  | *111.90                                | 11.75   | 112.20  | 1.84   | SE           |
| J1301+4803                  | 13:01:17.5             | +48:03:33               | 9018  | 8938   | 8.75 ± 0.89                                    |  | 361.96                                 | 6.86  | 52.78   | 8.57   | SS           |
| J1313+3910                  | 13:13:14.5             | +39:10:37               | 21475   | ...  | <4.70  |  | ...                                    | <3.01   | 83.18   | <0.68  | SE           |
| J1315+4424                  | 13:15:15.6             | +44:24:26               | 10740   | 10634  | 5.58 ± 0.63                                    |  | 352.93                                 | 10.16   | 163.35  | 10.63  | SS           |
| J1332-0301                  | 13:32:55.9             | -03:01:37               | 14643   | 14145  | 14.15 ± 1.89                                   | 10.18  | *165.80                                | 12.81   | 122.97  | 11.45  | SS           |
| J1346-0325                  | 13:46:21.1             | -03:25:23               | 7030  | 6883   | 4.40 ± 0.46                                    | 2.57   | *109.61                                | 2.82  | 48.98   | 0.28   | SE           |
| J1400-0254                  | 14:00:37.3             | -02:54:27               | 7390  | 7491   | 8.12 ± 0.87                                    |  | 669.25                                 | <1.09   | 75.29   | 0.08   | SS           |
| J1400+4251                  | 14:00:58.3             | +42:51:01               | 9939  | 9739   | 7.37 ± 0.79                                    |  | *418.83                                | 17.48   | 91.10   | 17.99  | SS           |
| J1405+6542                  | 14:05:52.1             | +65:42:43               | 9208  | 9224   | 5.45 ± 0.60                                    | 3.31   | *304.06                                | 6.31  | 19.95   | 0.73   | SE           |
| J1407-0234                  | 14:07:07.1             | -02:34:45               | 17020   | 16954  | 40.54 ± 4.29                                   |  | 659.52                                 | 10.23   | 95.50   | 1.49   | SE           |
| J1424-0304                  | 14:24:58.7             | -03:04:00               | 15400   | 15517  | 46.18 ± 4.73                                   |  | 702.46                                 | 17.36   | 213.11  | 4.07   | SS           |
| J1433+4004                  | 14:33:47.6             | +40:05:15               | 7871  | 7773   | 9.28 ± 0.95                                    | 8.67   | *269.16                                | 19.34   | 148.76  | 9.67   | SS           |
| J1500+4317                  | 15:00:24.4             | +43:17:04               | 9399  | 9046   | 14.65 ± 1.50                                   | 14.03  | 661.15                                 | <0.90   | 53.70   | <0.10  | SE           |
| J1510+5810                  | 15:10:16.8             | +58:10:39               | 9303  | ...  | <0.81  |  | ...                                    | 4.79  | 81.74   | 2.04   | SS           |
| J1523+3748                  | 15:23:38.3             | +37:48:44               | 7048  | ...  | <0.47  |  | ...                                    | 0.89  | 13.80   | 0.47   | SE           |
| J1526+5915                  | 15:26:48.3             | +59:15:47               | 13525   | ...  | <1.96  |  | ...                                    | <1.16   | 58.88   | <0.14  | SE           |
| J1528+4255                  | 15:28:14.7             | +42:56:13               | 5530  | 5473   | 8.54 ± 0.86                                    | 7.21   | *490.79                                | 8.42  | 141.32  | 3.07   | SS           |
| J1552+4620                  | 15:52:33.3             | +46:20:20               | 18060   | 17708  | 17.55 ± 1.93                                   |  | 554.70                                 | 14.45   | 83.18   | 3.53   | SE           |
| J1556+4757                  | 15:56:24.7             | +47:57:23               | 5850  | 5815   | 3.36 ± 0.35                                    | 2.89   | 831.43                                 | 2.34  | 14.12   | 1.50   | SE           |
| J1558+3227                  | 15:58:37.7             | +32:27:42               | 14679   | 14432  | 7.03 ± 0.85                                    |  | 342.53                                 | 10.89   | 113.93  | 4.81   | SS           |
| J1602+4111                  | 16:02:43.7             | +41:11:54               | 10026   | 10024  | 28.16 ± 2.84                                   | 27.45  | *490.18                                | 18.62   | 94.76   | 13.50  | SS           |
| J1614+3711                  | 16:14:54.2             | +37:11:10               | 17450   | 17541  | 34.27 ± 3.65                                   | 31.37  | 723.05                                 | <1.93   | 131.83  | 0.46   | SE           |
| J1635+2630                  | 16:35:43.3             | +26:30:49               | 21207   | 21191  | 60.97 ± 6.30                                   | 53.61  | *342.6                                 | <3.33   | 169.82  | 0.90   | SE           |
| J1637+4650                  | 16:37:26.7             | +46:50:10               | 17915   | 17398  | 16.29 ± 1.80                                   |  | *532.28                                | 31.34   | 277.47  | 3.73   | SS           |
| J1702+1859                  | 17:02:03.5             | +18:59:55               | 16965   | ...  | <2.61  |  | ...                                    | <1.71   | 46.77   | <0.31  | SE           |
| J1704+3448                  | 17:04:50.9             | +34:48:57               | 17028   | 16990  | 15.43 ± 1.71                                   |  | *348.13                                | 23.80   | 152.68  | 32.12  | SS           |

**Note.** — Descriptions of Columns: (1) Pair ID. The designations are “H-KPAIR J0118-0013”, etc. (2) R.A. (h:m:s, J2000). (3) decl. (d:m:s, J2000). (4) Optical velocity taken from SDSS or other telescopes. (5) HI mean velocity. (6) HI mass ( $10^9 M_{\odot}$ ). (7) HI mass after the correction of contamination due to neighboring galaxies ( $10^9 M_{\odot}$ ). (8) Linewidth measured at 20% of peak ( $\text{km s}^{-1}$ ); the symbol ‘\*’ denotes spectra with at least two kinematically resolved components, of which the  $W20$  is for the main component (the one with the highest integrated flux). (9) Dust mass multiplied by 100 ( $10^9 M_{\odot}$ ). The  $100 \times M_{\text{dust}}$  of S+S pairs with only one detection equals to that of the detected component. The  $100 \times M_{\text{dust}}$  of S+E pairs includes only that of spiral component. (10) Stellar mass ( $10^9 M_{\odot}$ ). The  $M_{\text{star}}$  of S+E pairs includes only that of spiral component. (11) Star formation rate ( $M_{\odot} \text{ yr}^{-1}$ ). The SFR of S+S pairs with only one detection equals to that of the detected component. The SFR of S+E pairs includes only that of spiral component. (12) Type of major-merger pairs.

**Table 2**  
Pairs from literatures.

| (1)        | (2)        | (3)       | (4)                    | (5)                  | (6)                          | (7)                  | (8)                             | (9)  | (10) | (11)               |
|------------|------------|-----------|------------------------|----------------------|------------------------------|----------------------|---------------------------------|------|------|--------------------|
| Pair ID    | R.A.       | decl.     | $V_{\text{HI}}$        | $M_{\text{HI}}$      | $100 \times M_{\text{dust}}$ | $M_{\text{star}}$    | SFR                             | Type | ref. | beam size          |
| (H-KPAIR)  | (J2000)    | (J2000)   | ( $\text{km s}^{-1}$ ) | ( $10^9 M_{\odot}$ ) | ( $10^9 M_{\odot}$ )         | ( $10^9 M_{\odot}$ ) | ( $M_{\odot} \text{ yr}^{-1}$ ) |      |      |                    |
| J0020+0049 | 00:20:27.4 | +00:49:59 | 5498                   | $3.30 \pm 0.49$      | 1.90                         | 31.24                | 1.39                            | SE   | 1    | 3.3'               |
| J0823+2120 | 08:23:32.6 | +21:20:16 | 5400                   | $12.12 \pm 1.17$     | 3.96                         | 33.79                | 3.98                            | SS   | 2    | 10.0'              |
| J0829+5531 | 08:29:15.0 | +55:31:21 | 7758                   | $25.59 \pm 2.65$     | 21.48                        | 85.47                | 3.98                            | SS   | 1    | 10.0'              |
| J1043+0645 | 10:43:51.9 | +06:46:00 | 8238                   | $6.70 \pm 0.27$      | 12.34                        | 59.98                | 5.01                            | SS   | 3    | $3.5' \times 3.8'$ |
| J1308+0422 | 13:08:28.3 | +04:22:01 | 7251                   | $8.26 \pm 0.26$      | 4.93                         | 23.58                | 0.66                            | SS   | 3    | $3.5' \times 3.8'$ |
| J1315+6207 | 13:15:34.6 | +62:07:28 | 9100                   | $5.00 \pm 0.83$      | 12.77                        | 103.90               | 62.89                           | SS   | 2    | 10.0'              |
| J1406+5043 | 14:06:21.7 | +50:43:29 | 1860                   | $1.63 \pm 0.17$      | 2.09                         | 13.92                | 0.92                            | SE   | 1    | 10.0'              |
| J1423+3400 | 14:23:42.5 | +34:00:30 | 3865                   | $1.03 \pm 0.10$      | 2.90                         | 25.92                | 1.23                            | SS   | 1    | 3.3'               |
| J1425+0313 | 14:25:05.5 | +03:13:59 | 10680                  | $1.50 \pm 0.35$      | < 1.02                       | 23.11                | < 0.10                          | SE   | 4    | 3.5'               |
| J1444+1207 | 14:44:20.7 | +12:07:55 | 8895                   | $5.93 \pm 0.64$      | 12.84                        | 186.60               | 4.64                            | SS   | 1    | 3.3'               |
| J1608+2328 | 16:08:22.5 | +23:28:46 | 12121                  | $14.87 \pm 1.50$     | 17.42                        | 71.43                | 12.19                           | SS   | 1    | 3.3'               |
| J2047+0019 | 20:47:19.0 | +00:19:17 | 4204                   | $22.44 \pm 3.45$     | 15.14                        | 123.10               | 1.84                            | SE   | 1    | 3.3'               |

**Note.** — Descriptions of Columns: (1) Pair ID. The designations are “H-KPAIR J0020+0049”, etc. (2) R.A. (h:m:s, J2000). (3) decl. (d:m:s, J2000). (4) HI velocity. (5) HI mass ( $10^9 M_{\odot}$ ). (6) Dust mass multiplied by 100 ( $10^9 M_{\odot}$ ). The  $100 \times M_{\text{dust}}$  of S+S pairs with only one detection equals to that of the detected component. The  $100 \times M_{\text{dust}}$  of S+E pairs includes only that of spiral component. (7) Stellar mass ( $10^9 M_{\odot}$ ). The  $M_{\text{star}}$  of S+E pairs includes only that of spiral component. (8) Star formation rate ( $M_{\odot} \text{ yr}^{-1}$ ). The SFR of S+S pairs with only one detection equals to that of the detected component. The SFR of S+E pairs includes only that of spiral component. (9) Type of major-merger pairs. (10) References: 1 [Springob et al. \(2005\)](#); 2 [Huchtmeier & Richter \(1989\)](#); 3 [Haynes et al. \(2011\)](#); 4 [Catinella et al. \(2010\)](#).

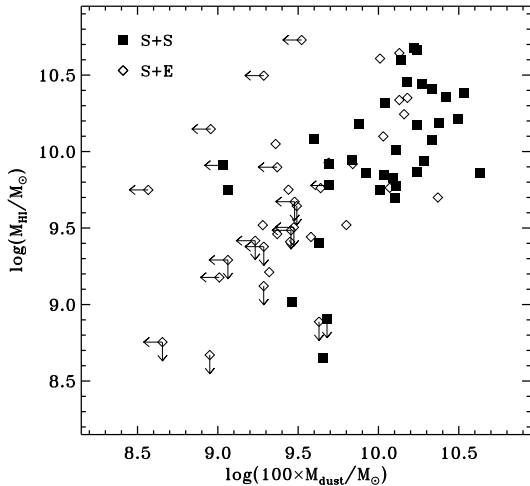


**Figure 2.** HI mass ( $M_{\text{HI}}$ ) vs.  $100 \times M_{\text{dust}}$  plot.

## 6. RESULTS

Our final sample includes 70 pairs (34 S+S pairs, 36 S+E pairs) whose HI mass  $M_{\text{HI}}$  can be found in Table 1 and Table 2. For S+S pairs, since the GBT beam cannot resolve them into individual galaxies, we treated each pair (including both components) as a single source. In these tables, we also listed  $100 \times M_{\text{dust}}$  as an estimate of total gas mass, stellar mass  $M_{\text{star}}$ , and SFR, all taken from Cao et al. (2016). The corresponding  $M_{\text{star}}$ ,  $100 \times M_{\text{dust}}$  and SFR for each S+S pair are sums of the two components. In cases that one of the two ( $100 \times M_{\text{dust}}$  or SFR) is undetected by *Herschel*, the true value for the pair should be limited between the detection and the sum of the detection plus the upper-limit of the undetected component. A test has shown that, for our statistical results (Table 3), the difference between calculations adopting either of these two limits is negligibly small (0.01-0.02 dex). We choose to take the detection as the value of the pair. For each S+E pair, we assumed that the HI mass is associated only with S component and contribution from the E component is negligible. We tested this assumption using the gas mass derived from the dust mass (Cao et al. 2016). We calculated the mean and error of the ratio of  $M_{\text{gas}}(\text{E})/M_{\text{gas}}(\text{S})$  using the K-M estimator (Kaplan & Meier 1958) which exploits the information in the upperlimits of  $M_{\text{gas}}(\text{E})$ . The result is  $0.11 \pm 0.01$ . This indicates that E galaxies contribute only 10% of the gas mass of S+E pairs, which is indeed negligible. Other variables, including  $M_{\text{star}}$ ,  $100 \times M_{\text{dust}}$  and SFR, are also for the S component only.

In Table 3, means and errors of  $\log[M_{\text{HI}}/(100 \times M_{\text{dust}})]$ ,  $\log(M_{\text{HI}}/M_{\text{star}})$ , and  $\log(\text{SFE}_{\text{HI}})$  are presented for the total sample of pairs and for the following three sets of contrasting sub-samples: (1) S+S vs. S+E; (2)  $\log(M_{\text{star}}/M_{\odot}) < 10.7$  vs.  $\log(M_{\text{star}}/M_{\odot}) > 10.7$  (for an S+S pair,  $M_{\text{star}}$  is the mean of the two components); (3) ‘‘JUS’’ vs. ‘‘INT & MER’’ pairs. According to Cao et al. (2016), ‘‘JUS’’ pairs are those without clear signs of interaction, ‘‘INT’’ and ‘‘MER’’ are pairs with signs of interaction and merging. In order to exploit information

in the upper limits, the calculations were carried out using the maximum likelihood Kaplan-Meier (K-M) estimator (Kaplan & Meier 1958). We derived the survival curves of these ratios through VOSTat (VOSTat Development Group 2013). The means and errors of statistical calculations are based on the integrated areas of the curves. The  $\log[M_{\text{HI}}/(100 \times M_{\text{dust}})]$  analysis is confined to sources (55) with  $M_{\text{dust}}$  detections, and the  $\log[\text{SFR}/M_{\text{HI}}]$  analysis to sources (58) with  $M_{\text{HI}}$  detections.

In Figure 2 we compare  $M_{\text{HI}}$  (contamination corrected) with  $100 \times M_{\text{dust}}$ . There is a good correlation between the two values, both probing the cold gas content in these pairs. The linear correlation coefficient is 0.53. For the Spearman’s rank correlation, the coefficient is 0.61 and the significance is  $2.60 \times 10^{-8}$ . The strong correlation suggests that a significant fraction of dust resides in HI gas, or the ratio between  $M_{\text{HI}}$  and  $M_{\text{H}_2}$  is relatively constant. For the total sample, the mean  $\log[M_{\text{HI}}/(100 \times M_{\text{dust}})] = -0.06 \pm 0.06$ . Cao et al. (2016) adopted  $100 \times M_{\text{dust}}$  as an estimate of the total gas mass  $M_{\text{gas}}$ . Taken at face value, our result indicates that the contribution of the HI gas to the total gas mass is  $87(\pm 12)\%$ . Draine et al. (2007) found an average dust-to-gas mass ratio of 0.007 for nearby spiral galaxies, corresponding to  $M_{\text{gas}}/M_{\text{dust}} = 143$ . Assuming this gas-to-dust mass ratio for our pairs, the contribution of the HI gas to the total gas mass would be  $61(\pm 9)\%$ .

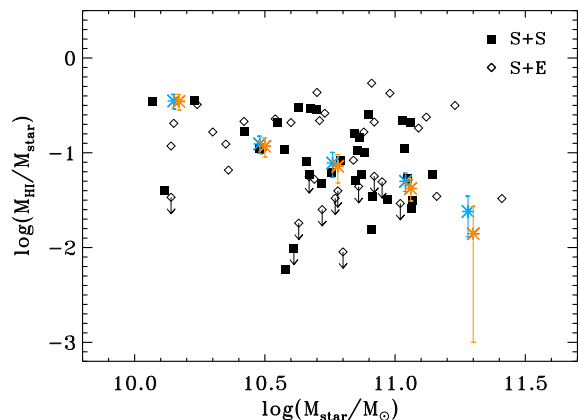


**Figure 3.** Plot of  $\log(M_{\text{HI}}/M_{\text{star}})$  vs.  $\log(M_{\text{star}})$ . For each S+E pair,  $M_{\text{star}}$  includes only the stellar mass of the spiral component. For each S+S pair, both the HI mass ( $M_{\text{HI}}$ ) and the total stellar mass ( $M_{\text{star}}$ ) of the pair are divided by 2. Results of Catinella et al. (2010) are shown by light blue 8-point stars (means derived assuming fluxes of undetected sources equal to the upperlimits) with error bars and by orange 8-point stars (means derived assuming fluxes of undetected sources equal to zero) with error bars.

In Figure 3, we plot  $\log(M_{\text{HI}}/M_{\text{star}})$  against  $\log(M_{\text{star}})$  for S+S and S+E pairs using different symbols. Since each S+S pair has two spirals while an S+E pair has only one, both  $M_{\text{HI}}$  and  $M_{\text{star}}$  of the former are divided by 2. The mean  $\log(M_{\text{HI}}/M_{\text{star}})$  ( $= -1.12 \pm 0.06$ ) for the total pair sample corresponds to a HI gas fraction of  $f_{\text{HI}} = 7.6(\pm 1.1)\%$ . More massive paired galaxies ( $M_{\text{star}} > 10^{10.7} M_{\odot}$ ) have a slightly lower average (mean  $\log(M_{\text{HI}}/M_{\text{star}}) = -1.13 \pm 0.07$ , corresponding to  $f_{\text{HI}} =$

7.4( $\pm 1.2$ )% compared with less massive paired galaxies of  $M_{\text{star}} < 10^{10.7} M_{\odot}$  which have mean  $\log(M_{\text{HI}}/M_{\text{star}}) = -1.06 \pm 0.11$  (corresponding to  $f_{\text{HI}} = 8.7(\pm 2.2)\%$ ). This is consistent with the results of [Catinella et al. \(2010\)](#) who showed that for a large sample of  $\sim 1000$  SFGs of  $10^{10} < M_{\text{star}} < 10^{11.5} M_{\odot}$ , there is a significant trend for the HI gas fraction to decrease with increasing  $M_{\text{star}}$ , with an overall average of  $f_{\text{HI}} \sim 10\%$  (Figure 3). We found no significant difference ( $< 1\sigma$ ) between the means of  $\log(M_{\text{HI}}/M_{\text{star}})$  of S+S and of S+E pairs (Table 3). This is different from [Cao et al. \(2016\)](#) who found, although with only marginal significance, that spirals in S+E pairs have on average lower total gas mass (estimated using the dust mass) to stellar mass ratio than those in S+S pairs.

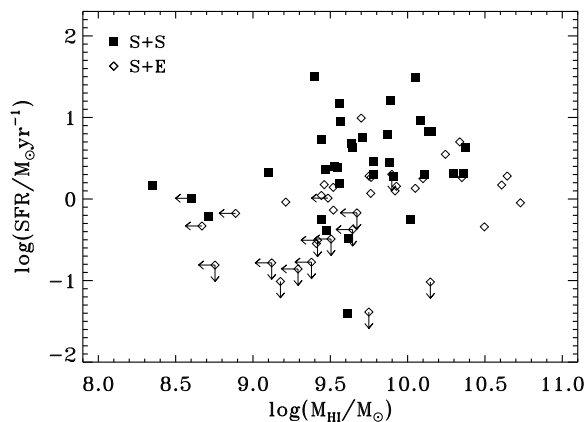


**Figure 4.** Plot of  $\log(\text{SFR})$  vs.  $\log(M_{\text{HI}})$ . For each S+E pair, SFR includes only that of the spiral component. For each S+S pair, both the HI mass ( $M_{\text{HI}}$ ) and the total SFR of the pair are divided by 2.

In Figure 4, we present  $\log(\text{SFR})$  vs.  $\log(M_{\text{HI}})$  plot for S+S and S+E pairs. Here again,  $M_{\text{HI}}$  and  $M_{\text{star}}$  of S+S pairs are divided by 2. There is a sub-population of very active star-forming galaxies (with  $\text{SFR} \gtrsim 10 M_{\odot} \text{ yr}^{-1}$ ) in S+S pairs. These galaxies are largely missing in S+E pairs.

In Figure 5,  $\log(\text{SFR})$  is plotted against HI gas fraction  $M_{\text{HI}}/M_{\text{star}}$ . It shows again that SFR of S+S pairs is systematically higher than that of S+E pairs. There is no clear dependence of SFR on HI gas fraction.

The ratio  $\text{SFR}/M_{\text{HI}}$  measures the star formation rate per unit HI gas mass, which will be referred as  $\text{SFE}_{\text{HI}}$  hereafter. In Figure 6,  $\log(\text{SFE}_{\text{HI}})$  is plotted against the HI gas fraction  $M_{\text{HI}}/M_{\text{star}}$ . It appears that for a given  $M_{\text{HI}}/M_{\text{star}}$ , the  $\text{SFE}_{\text{HI}}$  of S+E pairs is systematically lower than that of S+S pairs, and the difference is not sensitive to the HI fraction. As listed in Table 3, the mean  $\text{SFE}_{\text{HI}}$  of S+S pairs ( $10^{-9.26 \pm 0.11} \text{ yr}^{-1}$ ) is  $\sim 4.6\times$  higher than that of S+E pairs ( $10^{-9.92 \pm 0.11} \text{ yr}^{-1}$ ). There is a small but insignificant difference between the mean  $\text{SFE}_{\text{HI}}$  of pairs with signs of merger/interaction ( $10^{-9.45 \pm 0.14} \text{ yr}^{-1}$ ) and that of pairs without ( $10^{-9.60 \pm 0.09} \text{ yr}^{-1}$ ). The mean  $\text{SFE}_{\text{HI}}$  of the whole pair sample is  $10^{-9.55 \pm 0.09} \text{ yr}^{-1}$ , corresponding to a HI consumption time of  $3.5 \pm 0.7$  Gyrs.

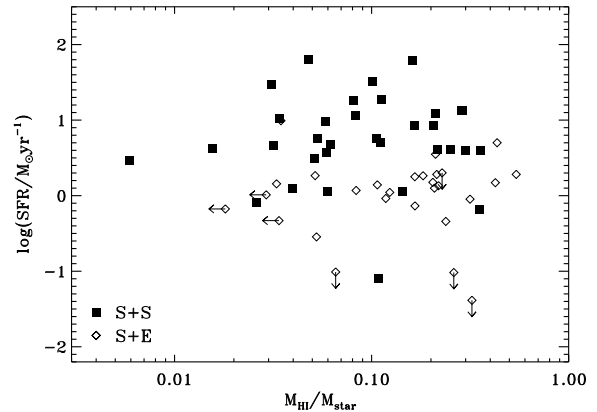


**Figure 5.** Plot of  $\log(\text{SFR})$  vs.  $M_{\text{HI}}/M_{\text{star}}$ .

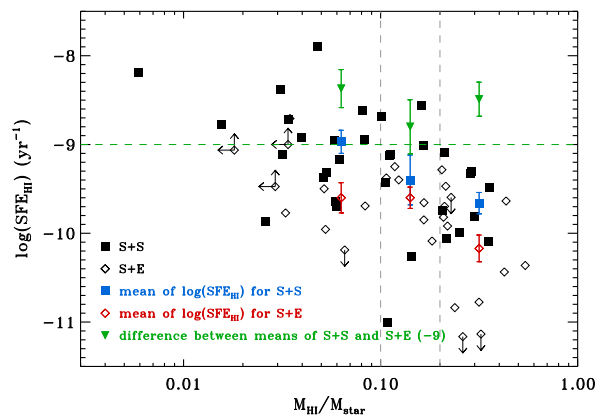


**Figure 6.** Plot of  $\log(\text{SFE}_{\text{HI}})$  vs.  $M_{\text{HI}}/M_{\text{star}}$ . The blue filled squares with error bars represent means of  $\log(\text{SFE}_{\text{HI}})$  of S+S pairs in HI fraction bins of  $M_{\text{HI}}/M_{\text{star}} < 0.1$ ,  $0.1 < M_{\text{HI}}/M_{\text{star}} < 0.2$ , and  $M_{\text{HI}}/M_{\text{star}} > 0.2$  for S+S pairs respectively. The red open diamonds with error bars are means for S+E pairs in the same bins. The vertical gray dashed lines at  $M_{\text{HI}}/M_{\text{star}} = 0.1$  and  $0.2$  mark the boundaries between the 3 bins. The green filled downward triangles represent the differences between the means of S+S pairs and that of S+E pairs. The green dashed line at  $-9$  of  $\log(\text{SFE}_{\text{HI}})$  represents the zero level of the differences.

## 7. DISCUSSION

Given the large beam ( $\text{FWHM} = 9'$ ) of theGBT observations, the HI detected for each pair includes both gas inside the discs and the stripped gas in tidal features and debris. Because of the exclusion of mergers with component separation less than 5 kpc and nearby pairs with recession velocity less than  $2000 \text{ km s}^{-1}$ , the H-KPAIR sample preferentially selects massive ( $\gtrsim 10^{10} M_{\odot}$ ) early stage merger systems (before the final coalescence). Our observations show that these systems have similar HI gas fractions compared to normal spiral galaxies (Figure 3). For gas-rich dwarf galaxy pairs  $M_{\text{star}} < 10^{9.7} M_{\odot}$ , [Stierwalt et al. \(2015\)](#) reached similar results. On the other hand, spiral galaxies in compact groups are found to be HI deficient ([Verdes-Montenegro et al. 2001](#); [Borthakur et al. 2015](#); [Walker et al. 2016](#)).

A major science goal of this study is to address the puzzling result of the significant difference between the



**Table 3**  
Kaplan-Meier estimation results.

| (1)<br>Samples                | (2)<br>$\log[M_{\text{HI}}/(100 \times M_{\text{dust}})]$ | (3)<br>Error | (4)<br>Count | (5)<br>$\log(M_{\text{HI}}/M_{\text{star}})$ | (6)<br>Error | (7)<br>Count | (8)<br>$\log(\text{SFR}/M_{\text{HI}})$ | (9)<br>Error | (10)<br>Count |
|-------------------------------|---|--------------|--------------|--|--------------|--------------|---|--------------|---------------|
| S+S                           | -0.09   | 0.07         | 32           | -1.09  | 0.08         | 34           | -9.26                                   | 0.11         | 33            |
| S+E                           | 0.002   | 0.08         | 23           | -1.01  | 0.07         | 36           | -9.92                                   | 0.11         | 25            |
| $\log M_{\text{star}} < 10.7$ | -0.12   | 0.10         | 23           | -1.06  | 0.11         | 28           | -9.59                                   | 0.14         | 24            |
| $\log M_{\text{star}} > 10.7$ | -0.02   | 0.06         | 32           | -1.13  | 0.07         | 42           | -9.53                                   | 0.12         | 34            |
| JUS                           | -0.05   | 0.09         | 28           | -1.10  | 0.10         | 34           | -9.60                                   | 0.09         | 29            |
| INT & MER                     | -0.07   | 0.07         | 27           | -1.11  | 0.07         | 36           | -9.45                                   | 0.14         | 29            |
| Total                         | -0.06   | 0.06         | 55           | -1.12  | 0.06         | 70           | -9.55                                   | 0.09         | 58            |

**Note.** — Descriptions of Columns: (1) Samples. (2) Means of  $\log[M_{\text{HI}}/(100 \times M_{\text{dust}})]$  ( $\log[(100 \times M_{\text{dust}})/M_{\text{HI}}]$  for comparison sample). (5) Means of  $\log(M_{\text{HI}}/M_{\text{star}})$ . (8) Means of  $\log(\text{SFR}/M_{\text{HI}})$ , the units are  $\text{yr}^{-1}$ . (3), (6) and (9): Errors of the means. (4), (7) and (10): Number of pairs in the calculation of the mean.

sSFR enhancement of spirals in S+E pairs and in S+S pairs (Xu et al. 2010; Cao et al. 2016). Because all pairs were selected using the same criteria regardless of morphological type (Domingue et al. 2009; Cao et al. 2016), this difference cannot be due to any selection bias. One possibility is that the sSFR in a paired galaxy is influenced by the immediate surrounding environment. This hypothesis is in agreement with the correlation between sSFRs of the primaries and secondaries in major-merger S+S pairs (i.e., the ‘‘Holmberg effect’’ Kennicutt et al. 1987; Xu et al. 2010). On the other hand, Xu et al. (2010, 2012) did not find any significant difference between the local densities around S+E pairs and S+S pairs within projected radius of 2 Mpc. Therefore, the linear scale of the environment effect must be less than 2 Mpc. Xu et al. (2010, 2012) speculated that the IGM in the dark matter halo (DMH) shared by both galaxies of a pair may play a significant role here. For example, when a DMH has strong (weak) cold flows (Dekel et al. 2009; Kereš et al. 2009), galaxies inside it may have abundant (scarce) cold gas supply to fuel active star formation. A prediction of this hypothesis is that spiral galaxies in S+E pairs have systematically lower gas content than those in S+S pairs.

However, this is not supported by our result which shows no significant difference between the mean  $\log(M_{\text{HI}}/M_{\text{star}})$  of S+S and that of S+E pairs. It appears that the higher sSFR and  $\text{SFE}_{\text{HI}}$  of S+S pairs are mainly due to a sub-population of very active SFGs, which are missing in S+E pairs (Figure 4). It will be very interesting to find out how the high star formation enhancement in these pairs is triggered, and why it is not happening in S+E pairs.

Some insights can be gained from the examples studied by Hibbard et al. (2001) using high resolution VLA HI maps for galaxies in the ‘‘merger sequence’’. Three of the five systems in their sample are early stage mergers with active star formation. They all show very extended tidal features in the HI gas distribution. However, most active star formation is confined to the central region where high density molecular gas and bright  $\text{H}\alpha$  emission are found. Dynamical simulations of Olson & Kwan (1990) demonstrated that, in the central  $\sim 2$  kpc of merging galaxies, interaction induced collisions between gas clouds may play very important roles in triggering enhanced star formation, and the effect is stronger in S+S systems than in S+E systems.

Scudder et al. (2015) carried out VLA observations (beam FWHM =  $14''$ ) of the HI 21 cm line emission

for 34 galaxies in 17 nearby S+S pairs, and obtained 17 detections. Compared to a control sample of galaxies, they found marginal evidence (at  $\sim 2\sigma$  level) for a positive correlation between the HI fraction and the SFR enhancement. On the other hand, Cao et al. (2016) did not see any significant correlation between  $\text{SFR}/M_{\text{gas}}$  enhancement and gas fraction in H-KPAIR. Our results in Figure 5 (Figure 6) show also that the difference between SFR ( $\text{SFE}_{\text{HI}}$ ) of spirals in S+S and S+E pairs does not depend on HI gas fraction.

## 8. SUMMARY

In this paper we present a study of the HI gas content of a large K-band selected sample of galaxy pairs (H-KPAIRs). Among 88 pairs (44 S+S pairs, 44 S+E pairs), we observed 67 pairs using GBT for the 21 cm HI fine-structure emission. Except for 9 pairs that have severe RFIs and thus no informative signals could be extracted from the data, we derived HI mass from the spectral line. The results include detections (46 pairs) and upper limits (12 pairs). In addition, HI mass of other 12 pairs are collected from the literature. Compared with the *Herschel* data of the same sample, the relations between  $M_{\text{HI}}$  and  $100 \times M_{\text{dust}}$ ,  $M_{\text{HI}}$  and SFR,  $M_{\text{HI}}$  and  $M_{\text{star}}$  and  $\text{SFE}_{\text{HI}}$  and HI fraction are studied. The means and errors of  $\log[M_{\text{HI}}/(100 \times M_{\text{dust}})]$ ,  $\log(M_{\text{HI}}/M_{\text{star}})$ , and  $\log(\text{SFE}_{\text{HI}})$  are derived and analyzed for the total sample and for three sets of contrasting sub-samples. The primary results are as follows.

- 1. Both linear and Spearman rank correlation analyses show a significant correlation between  $M_{\text{HI}}$  and  $100 \times M_{\text{dust}}$ . For the total sample, the mean  $\log[M_{\text{HI}}/(100 \times M_{\text{dust}})] = -0.06 \pm 0.06$ , corresponding to a HI-to-total gas ratio of  $87(\pm 12)\%$  if the gas-to-dust mass ratio is assumed as 100.
- 2. The mean HI-to-stellar mass ratio of spirals in these pairs is  $0.076 \pm 0.011$ , consistent with the average HI gas fraction of spiral galaxies in general. There is no significant difference ( $< 1\sigma$ ) between the means of  $\log(M_{\text{HI}}/M_{\text{star}})$  of S+S and of S+E pairs (Table 3).
- 3. The mean  $\text{SFE}_{\text{HI}}$  of S+S pairs ( $10^{-9.26 \pm 0.11} \text{ yr}^{-1}$ ) is  $\sim 4.6 \times$  higher than that of S+E pairs ( $10^{-9.92 \pm 0.11} \text{ yr}^{-1}$ ), and the difference is not sensitive to the HI fraction. A sub-population of very active star-forming galaxies in S+S pairs are largely missing in S+E pairs.

- : 4. The difference between the mean  $SFE_{\text{HI}}$  of pairs with signs of merger/interaction ( $10^{-9.45 \pm 0.14} \text{ yr}^{-1}$ ) and that of pairs without ( $10^{-9.60 \pm 0.09} \text{ yr}^{-1}$ ) is insignificant ( $< 1\sigma$ ).
- : 5. The mean  $SFE_{\text{HI}}$  of the whole pair sample is  $10^{-9.55 \pm 0.09} \text{ yr}^{-1}$ , corresponding to a HI consumption time of  $3.5 \pm 0.7$  Gyrs.

This work is supported by National Key R&D Program of China No. 2017YFA0402600, Open Project Program of the Key Laboratory of FAST, NAOC, Chinese Academy of Sciences, National Natural Science Foundation of

China No. 11643003 and No. 11373038, and International Partnership Program of Chinese Academy of Sciences No. 114A11KYSB20160008. This work is sponsored in part by the Chinese Academy of Sciences (CAS), through a grant to the CAS South America Center for Astronomy (CASSACA) in Santiago, Chile.

UL acknowledges support by the research projects AYA2014-53506-P from the Spanish Ministerio de Economía y Competitividad, from the European Regional Development Funds (FEDER) and the Junta de Andalucía (Spain) grants FQM108. D. L. acknowledges support from "CAS Interdisciplinary Innovation Team" program. C. C. is supported by NSFC-11503013, NSFC-11420101002.

## APPENDIX

### APPENDIX A

In Figure A1, we present the full intensity spectra of 5 nearby normal galaxies NGC895, NGC2718, NGC3027, UGC10014, and NGC6140. HI observations and data reduction of these galaxies are the same as for the paired galaxies (Sections 3 & 4). The results are compared with literature data in Table A1. When there are more than one previous HI observation for a given galaxy, its literature data is chosen according the following order of preference: (1) the latest GBT observation, (2) the latest NRAO 91m observation, (3) the latest Arecibo observation, (4) the latest observation by other telescopes. The comparison shows a systematic difference on a  $\sim 15\%$  level, possibly due to a minor deviation in the calibration. This shall not significantly affect our main conclusions.

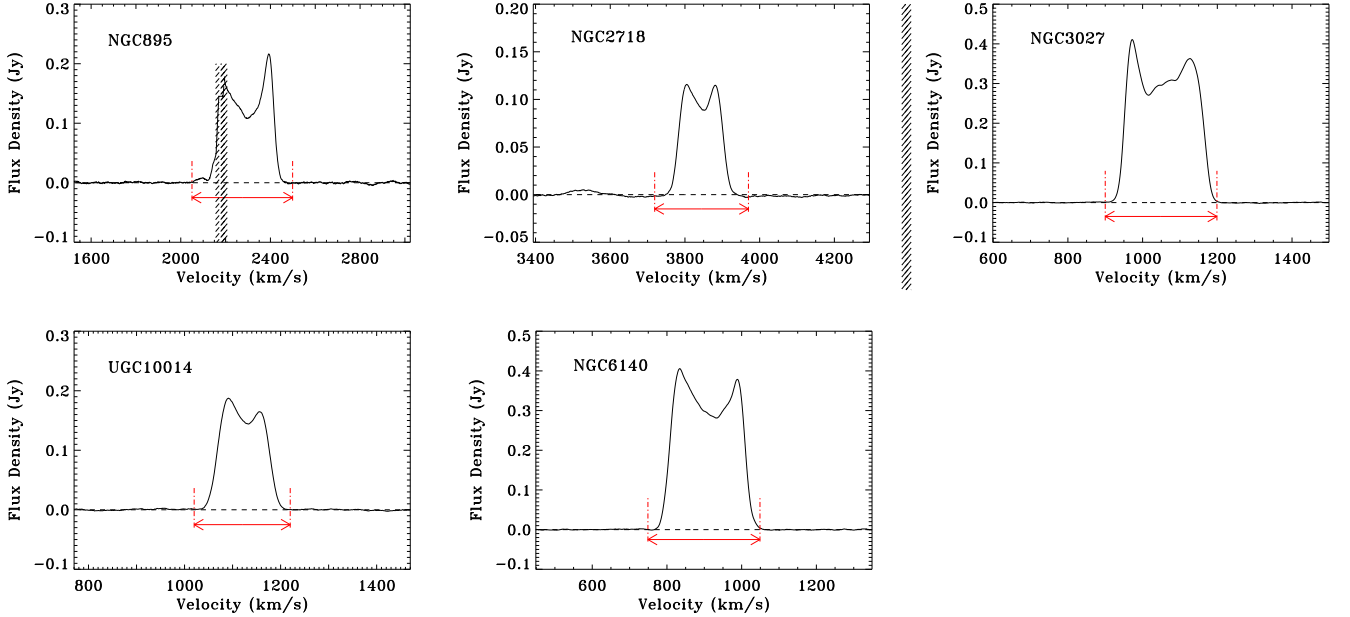


**Figure A1.** HI profiles of the normal galaxies observed with the 100-m GBT. Regions with hash marks are frequencies where data are affected by RFI spikes. The Region between two red dot-dash lines represents the range of the intensity flux integration.

### APPENDIX B

In this appendix, we present the algorithm of the correction for contaminations due to neighboring galaxies, and the postage stamp images (taken from SDSS-DR14) used in the correction (Figure B1).

In order to correct for the contamination, we estimated the HI mass of neighboring spiral galaxies using the following algorithm: First the HI-gas-to-stellar-mass ratio  $G_{\text{HI}}/S$  is estimated by  $\log_{10}(G_{\text{HI}}/S) = -1.73238(g-r) + 0.215182\mu_i - 4.08451$  (Zhang et al. 2009), where  $\mu_i$  is the  $i$ -band surface brightness and  $(g-r)$  is the optical colour derived from the  $g$ - and  $r$ -band Petrosian magnitudes. The surface brightness used here is defined as  $\mu_i = m_i + 2.5\log(2\pi R_{50}^2)$ , where  $m_i$  is the apparent Petrosian  $i$ -band magnitude and  $R_{50}$  the radius (in units of arcsecond) enclosing 50 percent of the total Petrosian  $i$ -band flux. Then the stellar mass was estimated from the  $i$ -band luminosity and  $g-r$  colour using the formula  $\log(M_*) = \log(L_i) - 0.222 + 0.864(g-r)$  (Bell et al. 2003). The estimated HI mass was then multiplied

**Table A1**  
Nearby normal galaxies in GBT observations.

| (1)       | (2)        | (3)       | (4)                    | (5)                    | (6)     | (7)     | (8)                       | (9)                       | (10)  | (11)       |
|-----------|------------|-----------|------------------------|------------------------|---------|---------|---------------------------|---------------------------|-------|------------|
| Galaxy ID | R.A.       | decl.     | $V_{\text{optical}}$   | $V_{\text{HI}}$        | $d_j$   | $d_i$   | $Sdv_{\text{HI}}$         | $Sdv_{\text{HI,ref}}$     | Dev.  | ref.       |
|           | (J2000)    | (J2000)   | ( $\text{km s}^{-1}$ ) | ( $\text{km s}^{-1}$ ) | ( $'$ ) | ( $'$ ) | ( $\text{Jy km s}^{-1}$ ) | ( $\text{Jy km s}^{-1}$ ) | (%)   |            |
| NGC895    | 02:21:36.5 | -05:31:17 | 2288                   | 2294                   | 3.6     | 2.6     | 33.39                     | 40.39                     | 18.98 | GBT100m(1) |
| NGC2718   | 08:58:50.5 | +06:17:35 | 3843                   | 3842                   | 1.74    | 0.91    | 13.07                     | 15.67                     | 18.09 | Arecibo(2) |
| NGC3027   | 09:55:40.6 | +72:12:13 | 1058                   | 1057                   | 4.3     | 2.0     | 71.72                     | 85.5                      | 17.53 | NRAO91m(3) |
| UGC10014  | 15:45:43.9 | +12:30:38 | 1121                   | 1121                   | 1.3     | 1.2     | 19.00                     | 21.2                      | 10.95 | GB91m(4)   |
| NGC6140   | 16:20:58.1 | +65:23:26 | 910                    | 906                    | 6.3     | 4.6     | 70.93                     | 84.6                      | 17.58 | NRAO91m(3) |

**Note.** — Descriptions of Columns: (1) Galaxy ID. (2) R.A. (h:m:s, J2000). (3) decl. (d:m:s, J2000). (4) Optical velocity taken from SDSS or other telescopes. (5) HI mean velocity. (6) The major diameter of the galaxy taken from NED. (7) The minor diameter of the galaxy taken from NED. (8) Integrated HI line flux of our observation. (9) Integrated HI line flux of literature data. (10) Relative difference between (8) and (9). (11) References of the literature data: 1 [Courtois et al. \(2009\)](#); 2 [Haynes et al. \(2011\)](#); 3 [Shostak \(1978\)](#); 4 [Tift & Cocke \(1988\)](#).

by the GBT beam response function at the distance of the galaxy, assuming the beam is a Gaussian with FWHM =  $9'$ . Finally, for each pair, the contamination due to HI mass of neighboring spiral galaxies so estimated was subtracted from its observed HI mass.

In Figure B1, postage stamp images taken from SDSS-DR14 are presented for individual pairs. In each image, paired galaxies are marked with yellow letters and neighboring galaxies with redshifts inside the bandwidth of the HI observation with green letters. For pairs with HI detections, the white circle represents the beam and the red circle the searching circle ( $r = 10'$ ). For pairs observed but undetected by GBT, only the beam circle is plotted. For pairs with bad data, neither circle is plotted. Besides, there are 9 pairs in galaxy groups and their HI observations were not pointed to the pairs, which are excluded from our analysis.

## REFERENCES

- Alonso, M. S., Tissera, P. B., Coldwell, G., & Lambas, D. G. 2004, *MNRAS*, 352, 1081
- Barton, E. J., Geller, M. J., & Kenyon, S. J. 2000, *ApJ*, 530, 660
- Bell, E. F., McIntosh, D. H., Katz, N., & Weinberg, M. D. 2003, *ApJS*, 149, 289
- Bergvall, N., Laurikainen, E., & Aalto, S. 2003, *A&A*, 405, 31
- Borthakur, S., Yun, M. S., Verdes-Montenegro, L., et al. 2015, *ApJ*, 812, 78
- Bushouse, H. A., Werner, M. W., & Lamb, S. A. 1988, *ApJ*, 335, 74
- Cao, C., Xu, C. K., Domingue, D., et al. 2016, *ApJS*, 222, 16
- Catinella, B., Schiminovich, D., Kauffmann, G., et al. 2010, *MNRAS*, 403, 683
- Condon, J. J., & Ransom, S. M. 2016, *Essential Radio Astronomy*
- Courtois, H. M., Tully, R. B., Fisher, J. R., et al. 2009, *AJ*, 138, 1938
- Dasyra, K. M., Tacconi, L. J., Davies, R. I., et al. 2006, *ApJ*, 638, 745
- Dekel, A., Birnboim, Y., Engel, G., et al. 2009, *Nature*, 457, 451
- Domingue, D. L., Cao, C., & Xu, C. K. e. a. 2016, *ApJ*, 829, 78
- Domingue, D. L., Xu, C. K., Jarrett, T. H., & Cheng, Y. 2009, *ApJ*, 695, 1559
- Draine, B. T., Dale, D. A., Bendo, G., et al. 2007, *ApJ*, 663, 866
- Ellison, S. L., Patton, D. R., Simard, L., & McConnell, A. W. 2008, *AJ*, 135, 1877
- Ellison, S. L., Patton, D. R., Simard, L., et al. 2010, *MNRAS*, 407, 1514
- Haynes, M. P., & Herter, T. 1988, *AJ*, 96, 504
- Haynes, M. P., Giovanelli, R., Martin, A. M., et al. 2011, *AJ*, 142, 170
- Hibbard, J. E., van der Hulst, J. M., Barnes, J. E., & Rich, R. M. 2001, *AJ*, 122, 2969
- Huchtmeier, W. K., & Richter, O.-G. 1989, *A General Catalog of HI Observations of Galaxies. The Reference Catalog.*, 350
- Hummel, E. 1981, *A&A*, 96, 111
- Kaplan, E. L., & Meier, P. 1958, *Journal of the American Statistical Association*, 53, 457
- Keel, W. C., Kennicutt, Jr., R. C., Hummel, E., & van der Hulst, J. M. 1985, *AJ*, 90, 708
- Kennicutt, Jr., R. C., Roettiger, K. A., Keel, W. C., van der Hulst, J. M., & Hummel, E. 1987, *AJ*, 93, 1011
- Kereš, D., Katz, N., Fardal, M., Davé, R., & Weinberg, D. H. 2009, *MNRAS*, 395, 160
- Lambas, D. G., Tissera, P. B., Alonso, M. S., & Coldwell, G. 2003, *MNRAS*, 346, 1189
- Larson, R. B., & Tinsley, B. M. 1978, *ApJ*, 219, 46
- Li, C., Kauffmann, G., Heckman, T. M., Jing, Y. P., & White, S. D. M. 2008, *MNRAS*, 385, 1903
- Marganian, P., Garwood, R. W., Braatz, J. A., Radziwill, N. M., & Maddalena, R. J. 2006, in *Astronomical Society of the Pacific Conference Series*, Vol. 351, *Astronomical Data Analysis Software and Systems XV*, ed. C. Gabriel, C. Arviset, D. Ponz, & S. Enrique, 512
- Nikolic, B., Cullen, H., & Alexander, P. 2004, *MNRAS*, 355, 874
- Olson, K. M., & Kwan, J. 1990, *ApJ*, 361, 426
- Patton, D. R., Torrey, P., Ellison, S. L., Mendel, J. T., & Scudder, J. M. 2013, *MNRAS*, 433, L59
- Sanders, D. B., & Mirabel, I. F. 1996, *ARA&A*, 34, 749
- Scudder, J. M., Ellison, S. L., Momjian, E., et al. 2015, *MNRAS*, 449, 3719
- Scudder, J. M., Ellison, S. L., Torrey, P., Patton, D. R., & Mendel, J. T. 2012, *MNRAS*, 426, 549
- Shostak, G. S. 1978, *A&A*, 68, 321
- Springob, C. M., Haynes, M. P., Giovanelli, R., & Kent, B. R. 2005, *VizieR Online Data Catalog*, 8077
- Stierwalt, S., Besla, G., Patton, D., et al. 2015, *ApJ*, 805, 2
- Sulentic, J. W. 1989, *AJ*, 98, 2066
- Telesco, C. M., Wolstencroft, R. D., & Done, C. 1988, *ApJ*, 329, 174
- Tift, W. G., & Cocke, W. J. 1988, *ApJS*, 67, 1
- Verdes-Montenegro, L., Yun, M. S., Williams, B. A., et al. 2001, *A&A*, 377, 812
- VOSTat Development Group. 2013, *VOSTat: Statistical analysis of astronomical data*, *Astrophysics Source Code Library*, ascl:1309.008
- Walker, L. M., Johnson, K. E., Gallagher, S. C., et al. 2016, *AJ*, 151, 30
- Xu, C., & Sulentic, J. W. 1991, *ApJ*, 374, 407
- Xu, C. K., Zhao, Y., Scoville, N., et al. 2012, *ApJ*, 747, 85
- Xu, C. K., Domingue, D., Cheng, Y.-W., et al. 2010, *ApJ*, 713, 330
- Zhang, W., Li, C., Kauffmann, G., et al. 2009, *MNRAS*, 397, 1243

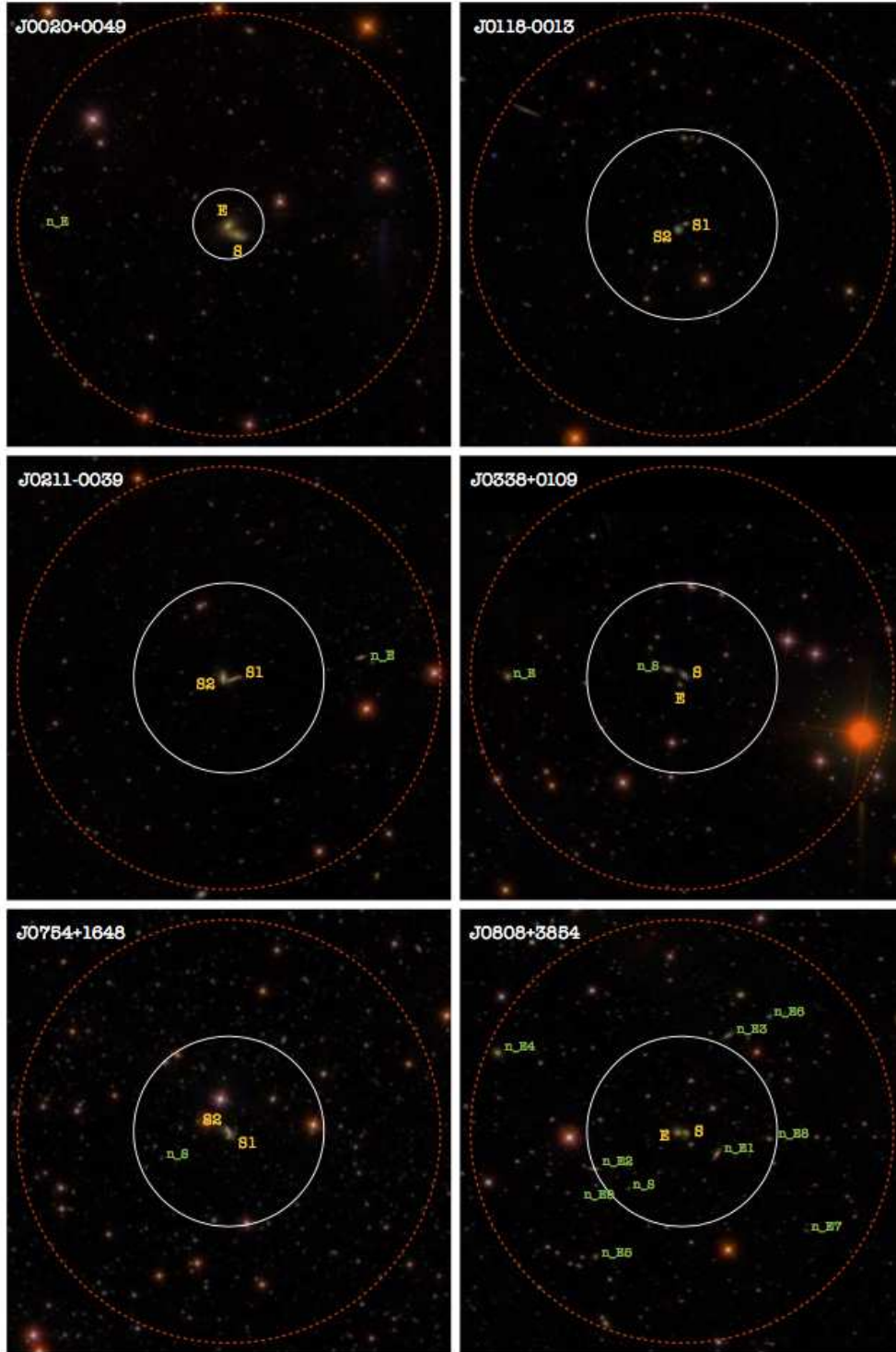


**Figure B1.** SDSS images of the 88 pairs. The white circles represent the FWHMs of the beams for the telescopes, which include GBT and the data from the literature (except for the bad data). The center of these circles are at the pointing position of the data. The red dashed line circles represent the search radius of 10' for the nearby galaxies. For S+E pairs, “S” and “E” are for the S and E components, respectively. For S+S pairs, “S1” represents the western galaxy and “S2” represents the eastern one. The nearby spirals and ellipticals are denoted by green n\_S1, n\_E1, n\_S2, n\_E2, ..., and only neighbors with redshift falling into the GBT bandpass. (The complete figure set (15 images) is available.)